Cross sections for vibronic excitation of CH^+ by low-energy electron impact

Xianwu Jiang [1], Chi Hong Yuen [2], Pietro Cortona,[1] Mehdi Ayouz [3], and Viatcheslav Kokoouline[2,*]

[1]*Laboratoire Structures, Propriétés et Modélisation des Solides de CentraleSupélec, CNRS-UMR8580, Université Paris-Saclay, 91190, Gif-sur-Yvette, France*

[2]*Department of Physics, University of Central Florida, 32816, Florida, USA*

[3]*Laboratoire Génie des Procédés et Matériaux EA 4038 de CentraleSupélec, Université Paris-Saclay, 91190, Gif-sur-Yvette, France*

(Received 26 September 2019; published 24 December 2019)

A theoretical approach for the electron-impact vibronic excitation of molecular ions with low-lying excited electronic states is described. In this approach, the fixed-nuclear *R*-matrix method is employed to compute electron-ion scattering matrices in the Born-Oppenheimer approximation. A vibronic frame transformation and the closed-channel elimination procedure in a spirit of molecular quantum defect theory are employed to construct an energy-dependent scattering matrix describing interactions between vibronic channels of the target ion induced by the incident electron. The obtained scattering matrix accounts for Rydberg series of vibronic resonances in the collisional spectrum. The approach is applied to the CH^+ ion of an astrophysical and technological interest. Cross sections for vibronic excitation for different combinations of initial and final vibronic states are computed. A good agreement between electronic-excitation cross sections, obtained using the quantum defect theory and in a direct *R*-matrix calculation, demonstrates that the present approach provides a reliable tool for determination of vibronic (de-)excitation cross sections for targets with low-energy electronic resonances. Such targets were difficult to treat theoretically using earlier methods.

DOI: 10.1103/PhysRevA.100.062711

I. INTRODUCTION

In many fields of research and applications, it is essential to have accurate cross sections for different processes taking place in collisions between molecular ions and electrons. Among such processes are electron-impact rotational (RE), vibrational (VE), and electronic (EE) excitation of the ions; dissociative recombination (DR); and photoionization and its inverse process, radiative recombination. Some cross sections could be obtained in experiments. However, for many processes, especially for the processes involving excited-state ions (ions here and below are assumed to be molecular ions, not atomic) or such ions as radicals, which are unstable in collisions with other species present nearby, an experimental approach is difficult or impossible. Even for stable ions in their ground quantum state, an experimental approach is often very expensive.

On the other hand, for theoretical approaches a significant complication in computation of the cross sections is the presence of vibrational and rotational degrees of freedom that have to be accounted for to obtain an accurate description of the processes. Electronic excitation and ionization of molecules can be treated theoretically, at least to some extent in the Born-Oppenheimer approximation or by taking into account the Franck-Condon factor. For other processes, such as rovibrational excitation or dissociative recombination, non-Born-Oppenheimer effects should be accounted for explicitly.

With modern development of electron-scattering methods and abundant computational resources, it became possible to compute, with an acceptable uncertainty, cross sections for many processes in electron-ion collisions. Significant progress was made for processes in diatomic ions formed by light elements: H_2^+ [1], HeH^+ [1], BeH^+ [2], BF^+ [3], CH^+ [4–7], SH^+ [8], N_2^+ [9–11], O_2^+ [12] with a few other diatomic ions, and the simplest triatomic ion H_3^+ with its isotopologs [13–17], where non-Born-Oppenheimer effects in electron-ion collisions were accurately accounted for, typically by using a quantum-defect approach combined with rotational and vibrational frame transformations. With some additional simplifications, such processes as rovibrational excitation and dissociative recombination were also successfully described theoretically for larger molecular ions: CH_3^+ [18], H_3O^+ [18,19], NH_4^+ [20], HCO^+ [21–27], BF_2^+ [28], N_2H^+ [27], $HCNH^+$ [29–32], $CH_2NH_2^+$ [33], and NH_2CHOH^+ [34].

Theoretically, non-Born-Oppenheimer couplings in electron-ion collisions are treated differently for the ions with low-energy electronic resonances appearing for geometries near the equilibrium of the target ion (in a fixed-nuclei picture) and for the ions without such low-energy electronic resonances. In the former case, usually the potential energy surface (PES) of the doubly excited neutral molecule crosses the ionic PES near the equilibrium geometry; in the latter case, there is no such a resonance PES. The ions of the first type usually (not always) have the first excited electronic state at a relatively low energy, below 5 eV; the ions of the second type have the first excited electronic state at a higher energy.

The presence of low-energy electronic resonances in the first type of the ions increases significantly compared to the ions of the second type, the DR, EE, VE, and RE cross sections at low collision energies. Because of the significant

*slavako@ucf.edu

difference in the physics of couplings in electron-ion collisions in the two types of the ions, one developed two types of approaches. The first approach, developed for DR, VE, and RE processes and originated from studies by O'Malley [35] and Bardsley [36–38], takes into account explicitly the PES crossing. The second approach, based mainly on studies by Lee [39], Jungen *et al.* [40,41], and Giusti [42] and employed when there is no PES crossing, accounts for the coupling between the incident electron and the rovibronic Rydberg resonances of the neutral molecule. In the absence of a PES crossing, such resonances are responsible for the major contribution to the DR cross section at low energies [13,42,43]. This is especially important for polyatomic ions, listed above. All these ions have a closed electronic shell, the first excited electronic state at a high energy, and no PES crossing near the equilibrium geometry of the ions.

There are situations where there is a PES crossing near the ion equilibrium geometry and, in addition, there are one or several low-energy electronic resonances in the collisional spectrum. Many open-shell ions are of this type, for example. The two approaches mentioned above are not able to describe satisfactory the DR and excitation processes. On the basis of an earlier theory suggested by Giusti [42,44], Jungen *et al.* have developed an efficient approach that can deal with such a situation. The approach was applied to several diatomic ions for which the dissociative electronic PES of the neutral molecule crosses the ionic PES near the ion equilibrium [6,45–47]. The approach is based on the quantum defect theory (QDT), where, in addition to one or several electronic states of the ion, the dissociative state is explicitly included into the coupling scheme [42,44]. Couplings between different electronic states of the target ion are derived from *ab initio* calculations of electronic (Rydberg) bound states of the neutral molecule. Couplings between the ionic and dissociative states are obtained from the autoionization widths of dissociative states of the neutral molecule (where autoionization is allowed). The widths are typically obtained in electron-scattering calculations.

The above theoretical approach is the only one able to describe non-Born-Oppenheimer effects on electron-ion collisions in the presence of coupled electronic channels of the target. One significant limitation of the approach is the difficulty in obtaining couplings between the electronic states. The procedure of diabatization of coupled Rydberg states obtained in *ab initio* calculations, used in the approach, is laborious, not unique, and sometimes not accurate. It becomes even more ambiguous and very complicated for polyatomic ions, such that an extension of the approach to polyatomic ions becomes impractical.

In this study, we propose another approach, which combines some of the original ideas from the molecular quantum defect theory [40,42,48], more recent DR and VE studies in polyatomic ions [14,21,25,27,43], and recent progress in electron-scattering calculations. The approach can be applied to determine EE, VE, RE, and DR cross sections for a wide range of small polyatomic ions, including the ions with one or several low-energy excited ionic and/or resonant states of the system. In this article, we focus on the VE process and, for the simplicity of discussion, on a particular case of a diatomic ion CH^+. However, the treatment can easily be applied to small polyatomic ions and, with some additions similar to Refs. [42,44], for the DR process.

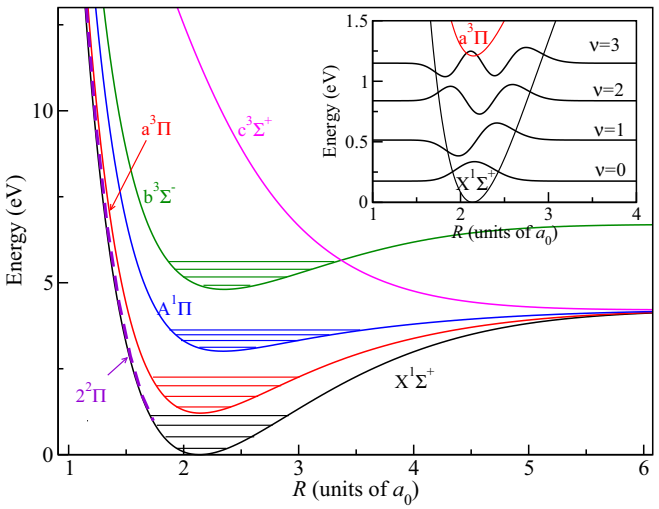

FIG. 1. Potential energy curves for the $X\,^1\Sigma^+$ (black curve), $a\,^3\Pi$ (red curve), $A\,^1\Pi$ (blue curve), $b\,^3\Sigma^-$ (green curve), and $c\,^3\Sigma^+$ (purple curve) electronic states of CH^+. Four lowest vibrational levels for the four lowest electronic states are shown by horizontal thin lines in potential wells of the states. The inset displays the four vibrational states $v = 0$–3 of the $X\,^1\Sigma^+$ state. The CH $2\,^2\Pi$ resonance state is plotted as thin dashed (violet) line. The CH $2\,^2\Pi$ resonance energies are obtained in fixed-nuclei R-matrix calculations at R varying from 1.137 to 1.737 bohrs with an interval of 0.1 bohrs.

II. ELECTRON-CH^+ COLLISIONS

Collisions of the CH^+ ion with electrons have been studied theoretically since, at least, 1951 [38,49–51]. The interest was motivated by the detection of the ion in diffuse interstellar clouds, made initially by Douglas and Herzberg [52] and by Adams [53] in 1941. These and later detections confirmed that CH^+ is ubiquitous as a major constituent of interstellar clouds. The ion is also an important intermediate in combustion and in the formation of large hydrocarbons in the interstellar medium (ISM). Reactive collisions of CH^+ with a low-energy electron determine the energy balance and evolution of low-temperature hydrocarbon plasmas such as in the ISM. The theoretical study of the e^--CH^+ collision system is thus of considerable astrophysical interest. Processes taking place in e^--CH^+ collisions are also of interest for technological plasmas: For example, they play an important role in plasma processing of diamond films [54] and at the edge plasma of fusion reactors [55], where graphite is used as plasma-facing material.

A theoretical description of low-energy e^--CH^+ collisions is complicated due to the presence of a low-energy electronic $2^2\Pi$ resonance and several low-energy excited electronic states of CH^+ [4,51,56] (see Fig. 1). The excited ionic states produce series of Rydberg resonances that influence all collisional processes. In this situation, the standard vibrational-frame-transformation approach by Chang and Fano [57], used in many theoretical studies on electron-molecule collisions [48,58], is not well adapted: The approach requires that

the scattering matrix or, alternatively, the matrix of quantum defects, obtained for fixed internuclear positions (in the Born-Oppenheimer approximation), to be a smooth function of the collision energy—ideally, to be energy independent. However, the presence of the $2\,^2\Pi$ resonance and the low-energy excited electronic states makes the fixed-nuclei scattering matrix to be strongly energy dependent.

The PES of the $2^2\Pi$ resonance crosses the PES of the ground electronic state $X\,^1\Sigma^+$ of the CH^+ ion slightly to the left of the CH^+ equilibrium geometry. As Giusti has pointed out [51], the electronic configuration of the resonance is mainly due to the coupling between the $3\sigma 1\pi(^1\Pi)4\sigma$ and $3\sigma 1\pi(^3\Pi)4\sigma$ orbitals of the $CH^+ + e^-$ system. The resonance at small internuclear distances has a Rydberg character and is produced by the $a\,^3\Pi$ and $A\,^1\Pi$ parent states of the CH^+ ion. These states are the first and second electronically excited states of the ion. Near and to the left of the crossing of the resonance and ionic $X\,^1\Sigma^+$ PES, the character of the resonance is mainly $3\sigma 1\pi(^1\Pi)4\sigma$ (see Fig. 1 of Ref. [51]). Therefore, the resonance could be included in the QDT description of the $CH^+ + e^-$ scattering if the $a\,^3\Pi$ and $A\,^1\Pi$ excited ionic states are accounted for in the complete scattering matrix. Of course, at low scattering energies at fixed geometries to the left of the crossing, these two electronic channels are closed for ionization and should be accounted for using the closed-channel elimination procedure [59], often employed in the QDT studies. Below, we describe in detail the developed theoretical approach.

III. QDT DESCRIPTION OF ELECTRONIC RESONANCES

In applications of the theoretical method presented below, one needs scattering matrices obtained numerically for fixed geometries of the target ion. The scattering matrices could be obtained in different ways. We used the UK R-matrix code [60]. The details of the numerical calculations using the R-matrix code for e^--CH^+ collisions are given in Sec. V.

As mentioned above, the geometry-fixed scattering matrix is strongly energy dependent for e^--CH^+ collisions. This is demonstrated in Fig. 2, showing derivatives of the eigenphase sums for the three symmetries $^2\Sigma^+$, $^2\Pi$, and $^2\Sigma^-$ of the e^--CH^+ system computed at the equilibrium with internuclear distance $R_e = 2.137$ bohrs. Several series of Rydberg resonances converge to the electronic states $a\,^3\Pi$ and $A\,^1\Pi$ as marked by the blue vertical lines in Fig. 2.

To describe low-energy electronic resonances in different e^--CH^+ scattering processes, we use the QDT approach and need an energy-independent scattering matrix, which includes not only the ground electronic state of CH^+ but a few more states that can produce resonances at scattering energies of the interest. In the e^--CH^+ case, low-energy resonances are well reproduced if one takes into account only three electronic states of the ion. Figure 2 shows derivatives of eigenphase sums in two calculations. In one calculation (black solid curves), only the three lowest $X\,^1\Sigma^+$, $a\,^3\Pi$, and $A\,^1\Pi$ states are included. In the second calculation (red dashed lines), 14 lowest states were included. As one can see, at low energies, below the $A\,^1\Pi$ ionization limit, the two calculations agree quite well with each other. In the second calculation with a larger number of ionic states, there are a few narrow

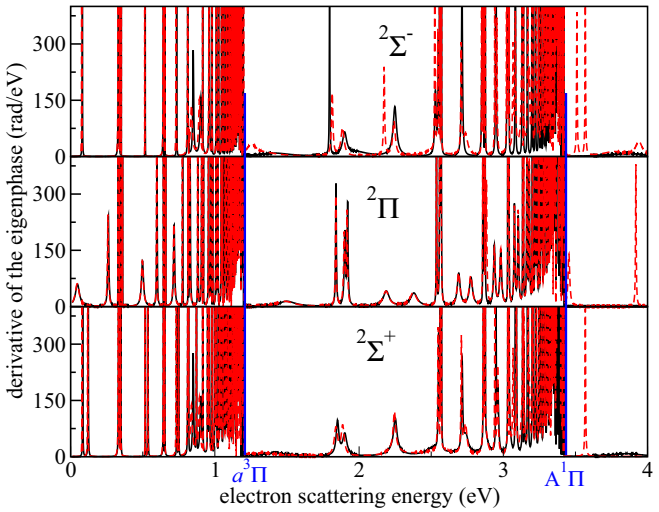

FIG. 2. Derivatives of the eigenphase sum for three symmetries $^2\Sigma^+$, $^2\Pi$, and $^2\Sigma^-$ of e^--CH^+ obtained for the equilibrium internuclear distance $R_e = 2.137$ bohrs in two different calculations: Black solid curves show the results obtained taking into account only three lowest electronic states of CH^+. Red dashed curves are obtained with 14 states. The differences between the curves are subtle and can hardly be seen in the figure.

resonances at low scattering energies that are not reproduced in the first, smaller calculation. These resonances are attached to very excited electronic states of the ion and do not influence significantly the low-energy spectrum.

Therefore, the electronic scattering matrix at low energies could well be represented by the three states $X\,^1\Sigma^+$, $a\,^3\Pi$, and $A\,^1\Pi$ of the ion. With this set of electronic states, the above-mentioned $2^2\Pi$ resonance is included in the scattering model.

In order to account for vibrational and rotational excitation of the target, the standard QDT approach is to use vibrational and rotational frame transformations [40,57]. The approach is applicable only if the electronic scattering matrix, obtained for a number of different geometries of the ion, is energy independent. As Fig. 2 shows, the e^--CH^+ scattering matrix depends strongly on energy below the $A\,^1\Pi$ ionization limit and cannot be immediately used in the frame transformation. A possible solution is to take the (almost) energy-independent scattering matrix, obtained at an energy above the $A\,^1\Pi$ ionization limit, and use it at energies below the limit. Therefore, the vibrational (and rotational) frame transformation is performed on a 3×3 electronic scattering matrix, which produces a $N \times N$ matrix with N vibronic (rovibronic) channels. Such a rovibronic scattering matrix is essentially energy independent and a QDT closed-channel elimination procedure [59,61] should be performed to obtain the physical energy-dependent matrix, which can be used to compute cross sections for various processes.

Before discussing the vibronic frame transformation applied to the e^--CH^+ collisions, we compare the fixed-nuclei electronic scattering matrices obtained (1) using the elimination procedure of the closed electronic states and by (2) a direct scattering R-matrix calculation at the same internuclear distance.

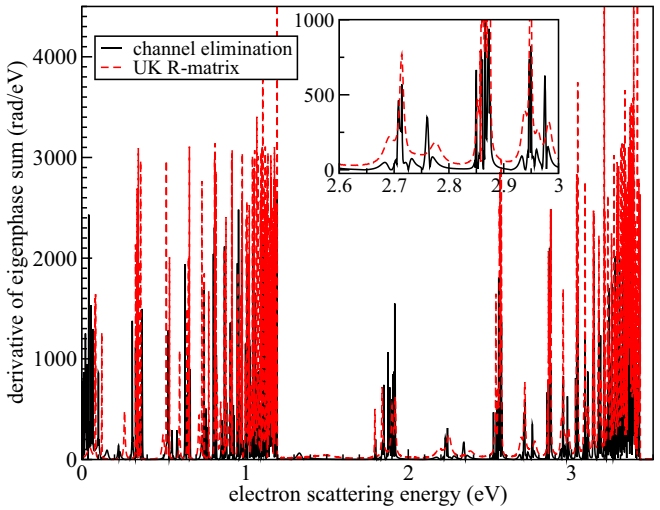

FIG. 3. Comparison of eigenphase-sum derivatives below the $A\,^1\Pi$ state obtained at a fixed CH^+ geometry in (1) the direct R-matrix calculations (red dashed curve) and using (2) the energy-independent 3×3 scattering matrix and the procedure of elimination of closed electronic channels (black solid curve). The inset shows an enlarged view for the 2.6- to 3.0-eV interval of energies.

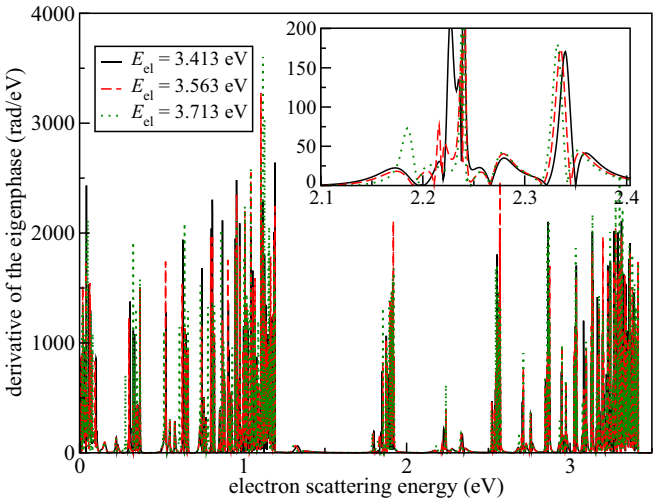

FIG. 4. Comparison of eigenphase-sum derivatives computed for a fixed CH^+ geometry using three different energy-independent 3×3 scattering matrices and the procedure of elimination of closed electronic channels. The three matrices are taken at energies 3.413 eV (black solid curve), 3.563 eV (red dashed curve), and 3.713 eV (green dotted curve). The inset shows an enlarged view for 2.1- to 2.4-eV energies.

The elimination of closed electronic channels at a geometry R is given by [59,61]

$$S^{\rm phys}(E_{\rm el}) = S^{oo} - S^{oc}[S^{cc} - e^{-2i\beta(E_{\rm el})}]^{-1}S^{co}\,, \qquad (1)$$

where $E_{\rm el}$ is the scattering energy and S^{oo}, S^{oc}, S^{cc}, and S^{co} are submatrices of the weakly dependent electronic scattering matrix (3×3 in the present case of the e^--CH^+ system),

$$S(E_{\rm el}) = \begin{pmatrix} S^{oo} & S^{oc} \\ S^{co} & S^{cc} \end{pmatrix}. \qquad (2)$$

Partition of matrix elements in the o and c parts is made on the basis of whether the corresponding channels are open or closed for excitation for the particular scattering energy $E_{\rm el}$. The quantity of $\beta(E_{\rm el})$ in Eq. (1) is a diagonal $N_c \times N_c$ matrix

$$\beta(E_{\rm el}, R) = \frac{\pi}{\sqrt{2[E_i(R) - E_{\rm el}]}}\delta_{i',i}, \qquad (3)$$

where $E_i(R)$ denotes the energy values of the ith electronic states at internuclear distance R.

Figure 3 shows derivatives of eigenphase sums obtained from the scattering matrices computed at the equilibrium distance R_e. The red dashed curve is the result from the R-matrix calculation; the black solid curve is the calculation using the energy-independent 3×3 electronic scattering matrix and the closed-channel elimination procedure. Overall, positions of the resonances in the two calculations are the same but widths in the R-matrix calculation are wider. This means that diagonal elements of the scattering matrices in the two calculations are very similar but the nondiagonal elements, responsible for channel couplings and widths of the resonances, are slightly different, suggesting that highly excited electronic states, neglected in the 3×3 channel elimination procedure, have non-negligible contributions to the coupling between the lowest channels.

The choice of the 3×3 scattering matrix used in the channel-elimination procedure is not unique, because the matrix depends on energy, even above the $A\,^1\Pi$ electronic state. To assess the result of uncertainty in the choice of the energy at which the 3×3 scattering matrix is taken, we plot in Fig. 4 eigenphase-sum derivatives obtained for 3×3 scattering matrices taken at three different energies above the $A\,^1\Pi$ state: at 3.413, 3.563, and 3.713 eV. Positions and the

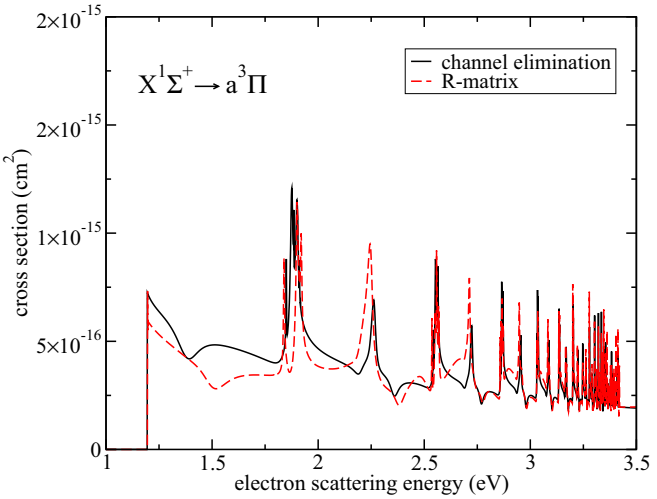

FIG. 5. Cross sections for the $X\,^1\Sigma^+ \rightarrow a\,^3\Pi$ electronic excitation of CH^+ at fixed geometry R_e obtained in the direct R-matrix calculations (red dashed curve) and using the QDT channel elimination procedure (black solid curve).

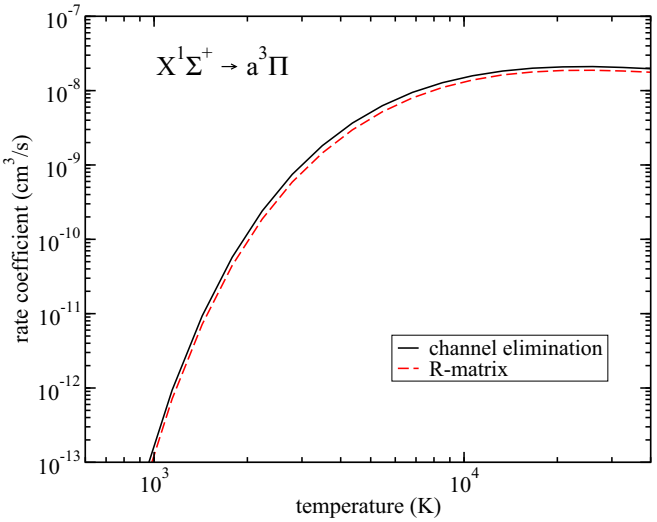

FIG. 6. The rate coefficients for the $X\,^1\Sigma^+ \rightarrow a\,^3\Pi$ electronic excitation of CH^+ at R_e obtained in the direct R-matrix calculations (red dashed curve) and the QDT channel elimination procedure (black solid curve).

widths of the resonances are nearly the same in the three calculations.

An important conclusion from the results discussed above is that the e^--CH^+ scattering physics below the $A\,^1\Pi$ state can be represented using an energy-independent multichannel scattering matrix evaluated at a higher energy, above the $A\,^1\Pi$ ionization limit in a combination with the closed-channel elimination.

A rough idea about the magnitude of cross sections for electron-impact electronic excitation of a molecule is obtained from a fixed-geometry calculation. Here, for a comparison between the QDT and direct R-matrix approaches, we present such excitation cross sections. The vibrational dynamics during the process is discussed in the next section.

Using the physical scattering matrix $S^{\rm phys}(E_{\rm el}, R_e)$ of Eq. (1) describing electronic transitions at the equilibrium geometry R_e of CH^+, the fixed-nuclei cross section of the electronic excitations from the $X\,^1\Sigma^+$ state to the $a\,^3\Pi$ state is computed in the QDT approach as [14]

$$\sigma_{i',i}(E_{\rm el}, R_e) = \frac{\pi\hbar^2}{2m_e E_{\rm el}} \times \sum_{l'm',lm} \left| S^{\rm phys}_{l'm'i',lmi}(E_{\rm el}, R_e) - \delta_{l'm'i',lmi} \right|^2, \quad (4)$$

where m_e is the reduced mass of electron and i and i' refer to the initial ($X\,^1\Sigma^+$ in this case) and final ($a\,^3\Pi$ here) electronic states. Indexes lm and $l'm'$ numerate initial and final angular momenta and their projections in the molecular reference frame (where *ab initio* calculations are performed). The cross section in the R-matrix approach is obtained by the same formula, except that the scattering matrix in the above equation is replaced with the one obtained directly in the R-matrix calculations at the corresponding energy $E_{\rm el}$.

Figure 5 compares the cross sections for the $X\,^1\Sigma^+ \rightarrow a\,^3\Pi$ transition obtained in the two approaches. The general agreement between the two curves is good, even for the widths of the resonances. One noticeable difference is in the position of the minimum near 1.5 eV: In the QDT calculations, it is shifted slightly to the left. The agreement is better at energies approaching the $a\,^3\Pi$ ionization limit.

Differences observed in the cross sections obtained by the two methods are smeared out in the thermally averaged rate coefficient

$$k_{i',i}(T, R_e) = \frac{8\pi}{(2\pi k_b T)^{3/2}} \int_0^\infty \sigma_{i',i}(E_{\rm el}, R_e) e^{\frac{-E_{\rm el}}{k_b T}} E_{\rm el} dE_{\rm el}, \quad (5)$$

computed from the cross sections. In the above equation, k_b is the Boltzmann coefficient and T is the temperature. The obtained rate coefficients, shown in Fig. 6, are in very good agreement with each other. This confirms that major couplings between electronic channels are accurately represented in the QDT approach and validates the approach.

IV. VIBRONIC EXCITATION

The energy-dependent physical scattering matrix for vibronic transitions is obtained in two steps. First, one computes the energy-independent vibronic scattering matrix assuming that all vibronic channels are open. In the second step, an

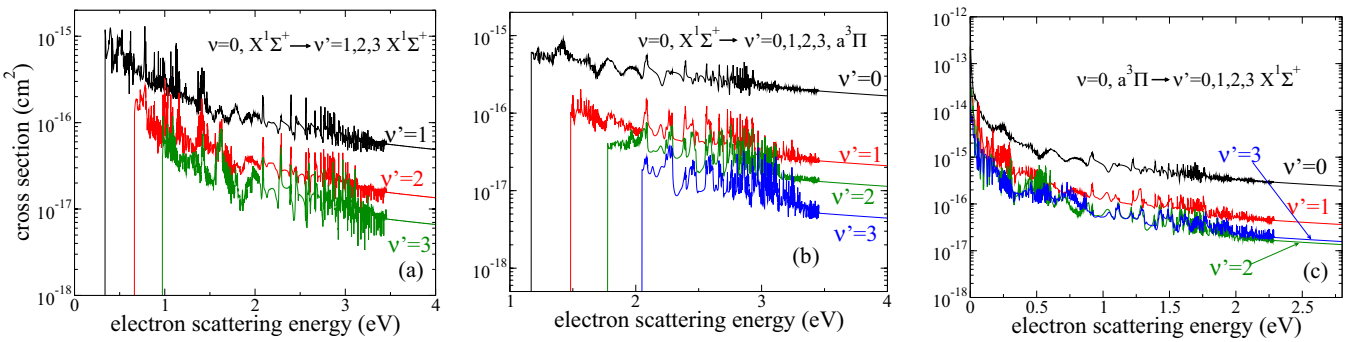

FIG. 7. Cross sections for vibronic excitations of CH^+ from the ground vibrational level $v = 0$ of the $X\,^1\Sigma^+$ state to $v = 1, 2, 3$ of the $X\,^1\Sigma^+$ state (left panel), to $v = 0, 1, 2, 3$ of the $a\,^3\Pi$ state (middle panel), and for vibronic de-excitations from the ground vibrational level $v = 0$ of $a\,^3\Pi$ to $v = 0, 1, 2, 3$ of the $X\,^1\Sigma^+$ state (right panel).

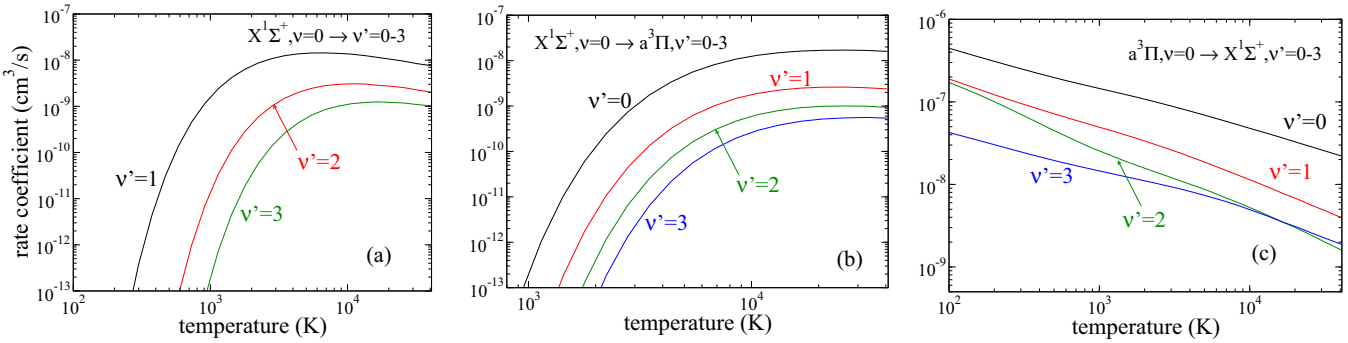

FIG. 8. Rate coefficients for same vibronic transitions as shown in Fig. 7.

elimination of closed vibronic channels is applied, producing the required energy-dependent vibronic scattering matrix.

The first step is performed by the vibronic frame transformation

$$S_{l'm'v'i',lmvi}(E_{\rm el}) = \langle \varphi_{v'i'}(R)|S_{l'm'i',lmi}(E_{\rm el},R)|\varphi_{vi}(R)\rangle, \quad (6)$$

where $\varphi_{vi}(R)$ and $\varphi_{v'i'}(R)$ are wave functions of the initial and final vibrational states. Index v or v' corresponds to the number of vibrational quanta in initial i or final i' electronic states. The brackets imply an integration over the vibrational coordinate R.

In the second step, the energy-dependent physical scattering matrix $S^{\rm phys}(E_{\rm el})$ is obtained by the QDT vibronic closed-channel elimination procedure, described by the same Eqs. (1) and (3), except that the energies $E_i(R)$ of closed channels are replaced with energies of vibronic channels E_{vi}, i.e.,

$$\beta(E_{\rm el}) = \frac{\pi}{\sqrt{2(E_{vi}-E_{\rm el})}}\delta_{v'i',vi}\,. \quad (7)$$

The cross sections $\sigma_{v'i',vi}(E_{\rm el})$ for vibronic excitation or de-excitation of CH^+ are computed using Eq. (4), where $S^{\rm phys}_{l'm'i',lmi}(E_{\rm el},R_{\rm e})$ is replaced with $S^{\rm phys}_{l'm'v'i',lmvi}(E_{\rm el})$.

Figure 7 illustrates cross sections obtained for different combinations of initial and final vibronic states. Figure 7(a) shows results for pure vibrational excitations between levels of the ground electronic state $X\,^1\Sigma^+$. As expected, the cross section for the transition with $\Delta v = 1$ is the largest one between inelastic processes. Figure 7(b) gives cross sections from the ground vibronic state $X\,^1\Sigma^+$, $v = 0$ to several vibrational levels of the $a\,^3\Pi$ state. Since the potential curves of the $X\,^1\Sigma^+$ and $a\,^3\Pi$ states have similar shapes near the equilibrium, the largest $X\,^1\Sigma^+ \to a\,^3\Pi$ cross section is expected to be for $\Delta v = 0$, as the present calculation indeed demonstrated. Figure 7(c) gives cross sections for the de-excitation process $a\,^3\Pi$, $v = 0 \to X\,^1\Sigma^+$, $v' = 0-3$.

Cross sections for vibronic excitations were recently estimated by Chakrabarti *et al.* [5] using a rough theoretical approach, in which cross sections for electronic excitations computed at the CH^+ equilibrium geometry were multiplied with Franck-Condon overlaps for various combinations of initial and final vibrational levels to obtain the cross sections for vibronic transitions. In that study, vibronic Feshbach resonances as well as differences in vibrational excitation energies were neglected. The cross sections obtained in Ref. [5] differ significantly—more than an order of magnitude for several transitions—from the present results. We attribute the disagreement to the mentioned approximations employed in Ref. [5]: (1) neglected differences in vibrational excitation threshold energies, (2) neglected dependence of e^--CH^+ scattering parameters with the internuclear distance, and (3) the neglected resonances in closed vibronic channels.

Thermally averaged rate coefficients $k_{v'i',vi}(T)$ for these vibronic (de-)excitations from 10 to 10 000 K are then computed using Eq. (5), where $\sigma_{i',i}(E_{\rm el},R_{\rm e})$ is substituted with $\sigma_{v'i',vi}(E_{\rm el})$. Figure 8 shows computed rate coefficients for the same transitions as the cross sections in Fig. 7.

As in previous studies [62–65] and for convenience of use, the computed thermally averaged rate coefficients $k_{v'i'\leftarrow vi}$ were fitted using the following analytical formula,

$$k^{\rm fit}_{v'i'\leftarrow vi}(T) = \frac{1}{\sqrt{T}}e^{-\frac{\Delta_{v'i',vi}}{T}}P^{\rm fit}_{v'i',vi}(x), \quad (8)$$

where $P^{\rm fit}_{v'i',vi}(x)$ is a quadratic polynomial

$$P^{\rm fit}_{v'i',vi}(x) = a_0 + a_1x + a_2x^2 \quad \text{and} \quad x = \ln(T) \quad (9)$$

with $P^{\rm fit}_{v'i',vi}(x) \approx P^{\rm fit}_{vi,v'i'}(x)$. This quantity could be viewed as the (de-)excitation probability. $\Delta_{v'i',vi}$ in Eq. (8) is the threshold energy defined as

$$\Delta_{v'i',vi} = \begin{cases} E_{v'i'} - E_{vi} > 0 & \text{for excitation,} \\ 0 & \text{for de-excitation.} \end{cases} \quad (10)$$

Numerically fitted parameters for vibronic transitions are given in Tables I–VI. When the parameters given in the tables are used in the fitting formulas of Eqs. (8) and (9) with T in K, obtained numerical values of rate coefficients will be in units

TABLE I. Parameters a_0, a_1, and a_2 of the polynomial $P^{\rm fit}_{vi,v'i'}(x)$ of Eqs. (8) and (9) for several pairs of initial and final vibrational levels of the ground electronic state $X\,^1\Sigma^+$ of CH^+. We specify the threshold energy $\Delta_{v'i',vi}$ for the excitation process in the pair $v'i'$, vi in the second column of each table. For the de-excitation process, $\Delta_{vi,v'i'} = 0$.

$v'i' \leftrightarrow vi$	$\Delta_{v'i',vi}$ (K)	a_0	a_1	a_2
10 ↔ 00	3 934	2.90×10^{-6}	-1.20×10^{-7}	2.30×10^{-9}
20 ↔ 00	7 700	1.10×10^{-6}	1.60×10^{-8}	-6.60×10^{-9}
30 ↔ 00	11 299	2.90×10^{-7}	5.00×10^{-8}	-5.10×10^{-9}
20 ↔ 10	3 766	7.85×10^{-7}	2.17×10^{-7}	-1.22×10^{-8}
30 ↔ 10	7 365	4.57×10^{-7}	1.02×10^{-7}	-8.64×10^{-9}
30 ↔ 20	3 599	2.39×10^{-6}	2.51×10^{-8}	-5.26×10^{-9}

TABLE II. Same as Table I for the electronic state $a\,^3\Pi$.

$v'i' \leftrightarrow vi$	$\Delta_{v'i',vi}$ (K)	a_0	a_1	a_2
$11 \leftrightarrow 01$	3 633	5.43×10^{-6}	4.68×10^{-7}	-4.41×10^{-8}
$21 \leftrightarrow 01$	7 039	2.01×10^{-6}	5.14×10^{-9}	-3.18×10^{-9}
$31 \leftrightarrow 01$	10 216	1.17×10^{-6}	-3.37×10^{-8}	-2.65×10^{-9}
$21 \leftrightarrow 11$	3 405	7.53×10^{-6}	6.95×10^{-8}	-2.30×10^{-8}
$31 \leftrightarrow 11$	6 583	2.99×10^{-6}	3.58×10^{-8}	-2.48×10^{-9}
$31 \leftrightarrow 21$	3 178	6.55×10^{-6}	2.04×10^{-7}	-8.40×10^{-9}

of cm^3/s. In the tables, the electronic states are numerated with index i (or i') with $i = 0$ corresponding to $X\,^1\Sigma^+$, $i = 1$ to $a\,^3\Pi$, and $i = 2$ to $A\,^1\Pi$.

V. CALCULATIONS OF ELECTRONIC STRUCTURE, SCATTERING, AND VIBRATIONAL DYNAMICS OF THE PROCESS

In this section, we provide details about numerical calculations of the vibrational wave functions of the ion and *ab initio* calculations performed for the bound electronic states of the ion and the e^--CH^+ scattering.

The configuration of the ground electronic state $X\,^1\Sigma^+$ of CH^+ is $1\sigma^2 2\sigma^2 3\sigma^2$ in the $C_{\infty v}$ symmetry group of the ion. The potential energy curves $V(R)$ of CH^+ were calculated using the C_{2v} symmetry group with a multireference configuration interaction (MRCI) method and the `cc-pV5Z` basis set using the MOLPRO code [66]. We kept the 1σ orbital of carbon doubly occupied and used 14 orbitals, i.e., 2σ-7σ, 1π-3π, and 1δ as the complete active space (CAS). The calculated potential energy curves of the $X\,^1\Sigma^+$, $a\,^3\Pi$, $A\,^1\Pi$, $b\,^3\Sigma^-$, and $c\,^3\Sigma^+$ electronic states are shown in Fig. 1. The $X\,^1\Sigma^+$, $a\,^3\Pi$, $A\,^1\Pi$, and $c\,^3\Sigma^+$ curves correlate with the $C^+(^2P) + H(^2S)$ dissociation limit at large internuclear distances.

In order to determine the vibrational energies E_v and the corresponding vibrational wave functions $\varphi_v(R)$ within these electronic states of CH^+, we solved the Schrödinger equation for vibrational motion along R

$$\left[-\frac{\hbar^2}{2\mu}\frac{d^2}{dR^2} + V(R)\right]\varphi_v(R) = E_v\varphi_v(R), \tag{11}$$

using a discrete variable representation (DVR) method [67]. In the above equation, μ denotes the reduced mass of CH^+. The lowest four vibrational energy levels $v = 0, 1, 2, 3$ of the $X\,^1\Sigma^+$ state are listed in Table VII. As one can see, the present computed energies agree well with the theoretical calculations by Biglari *et al.* [68].

TABLE III. Same as Table I for the electronic state $A\,^1\Pi$.

$v'i' \leftrightarrow vi$	$\Delta_{v'i',vi}$ (K)	a_0	a_1	a_2
$12 \leftrightarrow 02$	2 290	5.44×10^{-6}	1.74×10^{-7}	-1.09×10^{-8}
$22 \leftrightarrow 02$	4 271	2.16×10^{-6}	-1.24×10^{-8}	-6.08×10^{-10}
$32 \leftrightarrow 02$	5 971	1.49×10^{-6}	-8.82×10^{-9}	5.33×10^{-10}
$22 \leftrightarrow 12$	1 981	1.33×10^{-5}	-1.13×10^{-7}	-3.47×10^{-10}
$32 \leftrightarrow 12$	3 680	7.74×10^{-6}	8.39×10^{-9}	-8.35×10^{-10}
$32 \leftrightarrow 22$	1 699	3.48×10^{-6}	-1.17×10^{-8}	6.50×10^{-10}

TABLE IV. Same as Table I for vibronic transitions $vX\,^1\Sigma^+ \leftrightarrow v'a\,^3\Pi$.

$v'i' \leftrightarrow vi$	$\Delta_{v'i',vi}$ (K)	a_0	a_1	a_2
$01 \leftrightarrow 00$	13 572	5.10×10^{-6}	-1.20×10^{-8}	2.30×10^{-9}
$11 \leftrightarrow 00$	17 205	3.50×10^{-7}	2.70×10^{-7}	-2.20×10^{-8}
$21 \leftrightarrow 00$	20 610	5.00×10^{-7}	3.80×10^{-9}	-3.80×10^{-10}
$31 \leftrightarrow 00$	23 788	2.00×10^{-7}	5.70×10^{-8}	-5.70×10^{-9}
$01 \leftrightarrow 10$	9 638	4.90×10^{-7}	2.57×10^{-7}	-1.84×10^{-8}
$11 \leftrightarrow 10$	13 271	4.30×10^{-6}	5.30×10^{-8}	-2.80×10^{-9}
$21 \leftrightarrow 10$	16 677	7.13×10^{-7}	1.72×10^{-8}	-6.09×10^{-10}
$31 \leftrightarrow 10$	19 854	6.00×10^{-7}	1.98×10^{-8}	-5.12×10^{-10}
$01 \leftrightarrow 20$	5 872	7.06×10^{-7}	1.55×10^{-7}	-1.78×10^{-8}
$11 \leftrightarrow 20$	9 505	1.93×10^{-6}	-3.01×10^{-8}	-5.86×10^{-9}
$21 \leftrightarrow 20$	12 910	3.97×10^{-6}	-7.95×10^{-8}	6.09×10^{-9}
$31 \leftrightarrow 20$	16 088	9.13×10^{-7}	2.49×10^{-8}	-2.09×10^{-9}
$01 \leftrightarrow 30$	2 273	3.24×10^{-7}	4.24×10^{-8}	-2.23×10^{-9}
$11 \leftrightarrow 30$	5 906	8.23×10^{-7}	1.61×10^{-8}	-3.03×10^{-9}
$21 \leftrightarrow 30$	9 311	1.77×10^{-6}	-1.22×10^{-8}	-4.08×10^{-9}
$31 \leftrightarrow 30$	12 489	3.31×10^{-6}	-4.24×10^{-8}	3.17×10^{-10}

The e^--CH^+ scattering calculations were carried out using the UK R-matrix code [60,69] with the help of the Quantemol-N interface [70]. The `cc-pVQZ` basis set and CAS configuration interaction (CI) method in the C_{2v} Abelian subgroup were used in the calculations. The inner orbital $1a_1{}^2$ of CH^+ was frozen, and four external electrons were distributed in the space of the $[2a_1, 3a_1, 4a_1, 5a_1, 6a_1, 7a_1, 8a_1, 1b_1, 2b_1, 3b_1, 1b_2, 2b_2, 3b_2, 1a_2]$ orbitals ($2\sigma, 3\sigma, 4\sigma, 5\sigma, 6\sigma, 7\sigma, 1\pi, 2\pi, 3\pi, 1\delta$ in $C_{\infty v}$ symmetry group). We chose an R-matrix sphere of radius 13 bohrs and continuum Gaussian-type orbitals with partial waves $l \leqslant 4$. The two different R-matrix calculations described in Sec. III closed-coupling expansions with 3 and 14 lowest electronic states of CH^+ were used for constructing the total wave functions for the e^--CH^+ system. In the

TABLE V. Same as Table I for vibronic transitions $vX\,^1\Sigma^+ \leftrightarrow v'A\,^1\Pi$.

$v'i' \leftrightarrow vi$	$\Delta_{v'i',vi}$(K)	a_0	a_1	a_2
$02 \leftrightarrow 00$	34 147	3.30×10^{-6}	-2.10×10^{-7}	9.90×10^{-9}
$12 \leftrightarrow 00$	36 437	1.70×10^{-6}	-7.70×10^{-8}	2.90×10^{-9}
$22 \leftrightarrow 00$	38 418	6.70×10^{-7}	-1.20×10^{-8}	4.70×10^{-10}
$32 \leftrightarrow 00$	40 117	3.40×10^{-7}	-2.70×10^{-9}	1.50×10^{-10}
$02 \leftrightarrow 10$	30 213	1.21×10^{-6}	4.41×10^{-8}	-3.94×10^{-9}
$12 \leftrightarrow 10$	32 503	8.20×10^{-7}	-2.90×10^{-8}	-9.71×10^{-10}
$22 \leftrightarrow 10$	34 484	1.01×10^{-6}	2.69×10^{-9}	-3.61×10^{-10}
$32 \leftrightarrow 10$	36 183	7.74×10^{-7}	1.83×10^{-8}	-9.69×10^{-10}
$02 \leftrightarrow 20$	26 446	4.39×10^{-7}	2.69×10^{-8}	-1.11×10^{-9}
$12 \leftrightarrow 20$	28 737	1.17×10^{-6}	-2.14×10^{-8}	7.31×10^{-10}
$22 \leftrightarrow 20$	30 718	2.36×10^{-7}	8.67×10^{-10}	-5.88×10^{-11}
$32 \leftrightarrow 20$	32 417	3.82×10^{-7}	-5.63×10^{-9}	3.06×10^{-10}
$02 \leftrightarrow 30$	22 847	4.27×10^{-7}	-1.51×10^{-8}	-5.84×10^{-11}
$12 \leftrightarrow 30$	25 138	1.46×10^{-6}	2.16×10^{-8}	-2.89×10^{-9}
$22 \leftrightarrow 30$	27 119	7.21×10^{-7}	1.48×10^{-9}	-3.23×10^{-10}
$32 \leftrightarrow 30$	28 818	1.19×10^{-6}	-1.90×10^{-8}	1.04×10^{-9}

TABLE VI. Same as Table I for vibronic transitions $va\,^3\Pi \leftrightarrow v'A\,^1\Pi$.

$v'i' \leftrightarrow vi$	$\Delta_{v'i',vi}$ (K)	a_0	a_1	a_2
02 ↔ 01	20 575	3.28×10^{-6}	4.81×10^{-8}	-7.56×10^{-9}
12 ↔ 01	22 865	7.02×10^{-7}	2.32×10^{-9}	-1.11×10^{-9}
22 ↔ 01	24 846	5.83×10^{-7}	-4.73×10^{-9}	-2.56×10^{-11}
32 ↔ 01	26 545	4.43×10^{-7}	2.81×10^{-9}	-1.53×10^{-10}
02 ↔ 11	16 941	5.03×10^{-6}	2.61×10^{-7}	-1.85×10^{-8}
12 ↔ 11	19 232	1.08×10^{-6}	1.17×10^{-8}	-3.14×10^{-9}
22 ↔ 11	21 213	1.52×10^{-6}	-4.00×10^{-9}	-3.32×10^{-10}
32 ↔ 11	22 912	6.47×10^{-7}	-3.27×10^{-9}	1.69×10^{-10}
02 ↔ 21	13 536	1.39×10^{-6}	1.24×10^{-7}	-6.56×10^{-9}
12 ↔ 21	15 826	3.69×10^{-6}	-1.94×10^{-8}	9.08×10^{-10}
22 ↔ 21	17 807	7.26×10^{-7}	-2.50×10^{-8}	1.19×10^{-9}
32 ↔ 21	19 507	5.32×10^{-7}	6.38×10^{-9}	-3.78×10^{-10}
02 ↔ 31	10 358	1.30×10^{-6}	-9.89×10^{-8}	2.13×10^{-9}
12 ↔ 31	12 649	2.41×10^{-6}	7.13×10^{-8}	-5.00×10^{-9}
22 ↔ 31	14 630	1.54×10^{-6}	9.42×10^{-9}	-6.05×10^{-10}
32 ↔ 31	16 329	1.08×10^{-6}	-1.35×10^{-9}	4.25×10^{-11}

vibrational frame transformation of Eq. (6), the electron scattering calculations were performed in the interval between 1.537 and 3.937 bohrs with a step of 0.1 bohrs along the internuclear coordinate R.

VI. CONCLUSIONS

In conclusion, cross sections and rate coefficients for vibronic excitation and de-excitation of CH^+ by electron impact were computed in a framework using first principles only. The theoretical approach combines fixed-nuclei scattering matrices obtained for a number of internuclear distances using the UK R-matrix code, the vibronic frame transformation, and the QDT closed-channel elimination procedure. The approach is validated in model calculations for electronic excitation, performed for a single fixed internuclear distance of the target, comparing the results from a direct R-matrix calculation and the QDT channel elimination procedure. The main advantage of this method compared with the previous state of theory is that it can be applied to collisions of electrons with molecular ions with low-lying excited electronic states, including open-shell ions. The approach is quite general and can be applied for a number of different processes, taking place in collisions of molecular ions with electrons, including rovibronic excitation, dissociative excitation (DE), photoionization, and dissociative recombination (DR).

TABLE VII. Comparison of the four lowest vibrational energy levels (in eV) of the $X\,^1\Sigma^+$ state obtained in this study with the calculations by Biglari *et al.* [68].

Ref.	$v = 0$	$v = 1$	$v = 2$	$v = 3$
Biglari *et al.* [68]	0.175218	0.514360	0.838974	1.149288
This work	0.175189	0.514102	0.838515	1.148720
Relative error	0.017%	0.050%	0.055%	0.054%

In this study, we took into account only the electronic and vibrational structure of the target ion. The rotational structure of each vibrational level was neglected. The description of the rotational structure and couplings could be included into the treatment in the same way as was made in many previous treatments (see, for example, Ref. [65] and references therein). Therefore, the obtained cross sections and rate coefficients should be viewed as averaged over initial rotational states and summed over final rotational states of the corresponding vibrational levels. The inclusion of the rotational structure and couplings is important if one needs rotationally resolved cross sections or thermally averaged rate coefficients at temperatures T comparable or smaller than the CH^+ rotational constant, i.e., at $T \lesssim 20$ K. An extension of this method to include nuclear rotation will be discussed in a later publication.

ACKNOWLEDGMENTS

This work acknowledges support from the National Science Foundation, Grant No. PHY-1806915, China Scholarship Council, and the Thomas Jefferson Fund of the Office for Science and Technology of the Embassy of France in the United States. It has also received funding from the program "Accueil des chercheurs étrangers" of CentraleSupélec and "Séjour à l'étranger 2019" of École doctorale INTERFACES of Université Paris-Saclay.

[1] H. Takagi, Fusion Sci. Technol. **63**, 406 (2013).
[2] V. Laporta, K. Chakrabarti, R. Celiberto, R. Janev, J. Z. Mezei, S. Niyonzima, J. Tennyson, and I. Schneider, Plasma Phys. Controlled Fusion **59**, 045008 (2017).
[3] N. Pop, Z. Mezei, O. Motapon, S. Niyonzima, K. Chakrabarti, F. Colboc, R. Boată, M. D. E. Epée, and I. F. Schneider, AIP Conf. Proc. **1796**, 020014 (2017).
[4] L. Carata, A. E. Orel, M. Raoult, I. F. Schneider, and A. Suzor-Weiner, Phys. Rev. A **62**, 052711 (2000).
[5] K. Chakrabarti, A. Dora, R. Ghosh, B. Choudhury, and J. Tennyson, J. Phys. B: At., Mol. Opt. Phys. **50**, 175202 (2017).
[6] K. Chakrabarti, J. Z. Mezei, O. Motapon, A. Faure, O. Dulieu, K. Hassouni, and I. F. Schneider, J. Phys. B: At., Mol. Opt. Phys. **51**, 104002 (2018).
[7] Z. J. Mezei, M. D. Epée Epée, O. Motapon, and I. F. Schneider, Atoms **7**, 82 (2019).
[8] D. Kashinski, D. Talbi, A. Hickman, O. Di Nallo, F. Colboc, K. Chakrabarti, I. Schneider, and J. Z. Mezei, J. Chem. Phys. **146**, 204109 (2017).
[9] S. L. Guberman, J. Phys. Chem. A **111**, 11254 (2007).
[10] D. A. Little, K. Chakrabarti, J. Z. Mezei, I. F. Schneider, and J. Tennyson, Phys. Rev. A **90**, 052705 (2014).
[11] M. Fifirig, Mol. Phys. **112**, 1910 (2014).
[12] S. L. Guberman, Science **278**, 1276 (1997).
[13] V. Kokoouline, C. H. Greene, and B. D. Esry, Nature (London) **412**, 891 (2001).
[14] V. Kokoouline and C. H. Greene, Phys. Rev. Lett. **90**, 133201 (2003).

[15] S. Fonseca dos Santos, V. Kokoouline, and C. H. Greene, J. Chem. Phys. **127**, 124309 (2007).
[16] L. Pagani, C. Vastel, E. Hugo, V. Kokoouline, C. H. Greene, A. Bacmann, E. Bayet, C. Ceccarelli, R. Peng, and S. Schlemmer, Astron. Astrophys. **494**, 623 (2009).
[17] C. Jungen and S. T. Pratt, Phys. Rev. Lett. **102**, 023201 (2009).
[18] N. Douguet, A. E. Orel, C. H. Greene, and V. Kokoouline, Phys. Rev. Lett. **108**, 023202 (2012).
[19] N. Douguet, A. Orel, I. Mikhailov, I. F. Schneider, C. H. Greene, and V. Kokoouline, J. Phys. Conf. Ser. **300**, 012015 (2011).
[20] N. Douguet, V. Kokoouline, and A. E. Orel, J. Phys. B: At. Mol. Opt. Phys. **45**, 051001 (2012).
[21] I. A. Mikhaylov, V. Kokoouline, A. Larson, S. Tonzani, and C. H. Greene, Phys. Rev. A **74**, 032707 (2006).
[22] N. Douguet, V. Kokoouline, and C. H. Greene, Phys. Rev. A **77**, 064703 (2008).
[23] C. Jungen and S. T. Pratt, J. Chem. Phys. **129**, 164311 (2008).
[24] N. Douguet, V. Kokoouline, and C. H. Greene, Phys. Rev. A **80**, 062712 (2009).
[25] C. Jungen and S. T. Pratt, J. Chem. Phys. **133**, 214303 (2010).
[26] V. Kokoouline, N. Douguet, and C. H. Greene, Chem. Phys. Lett. **507**, 1 (2011).
[27] S. Fonseca dos Santos, N. Douguet, V. Kokoouline, and A. E. Orel, J. Chem. Phys. **140**, 164308 (2014).
[28] V. Kokoouline, M. Ayouz, J. Z. Mezei, K. Hassouni, and I. F. Schneider, Plasma Sources Sci. Technol. **27**, 115007 (2018).
[29] A. Hickman, R. Miles, C. Hayden, and D. Talbi, Astron. Astrophys. **438**, 31 (2005).
[30] V. Ngassam, A. E. Orel, and A. Suzor-Weiner, J. Phys. Conf. Ser. **4**, 224 (2005).
[31] V. Ngassam and A. E. Orel, Phys. Rev. A **75**, 062702 (2007).
[32] N. Douguet, S. F. dos Santos, V. Kokoouline, and A. Orel, EPJ Web Conf. **84**, 07003 (2015).
[33] C. Yuen, M. Ayouz, N. Balucani, C. Ceccarelli, I. Schneider, and V. Kokoouline, Mon. Not. R. Astron. Soc. **484**, 659 (2019).
[34] M. Ayouz, C. Yuen, N. Balucani, C. Ceccarelli, I. Schneider, and V. Kokoouline, Mon. Not. R. Astron. Soc. **490**, 1325 (2019).
[35] T. F. O'Malley, Phys. Rev. **150**, 14 (1966).
[36] J. N. Bardsley, J. Phys. B: At. Mol. Phys. **1**, 365 (1968).
[37] J. Bardsley, J. Phys. B: At. Mol. Phys. **1**, 349 (1968).
[38] J. Bardsley and B. Junker, Astrophys. J. **183**, L135 (1973).
[39] C. M. Lee, Phys. Rev. A **16**, 109 (1977).
[40] C. Jungen and O. Atabek, J. Chem. Phys. **66**, 5584 (1977).
[41] Ch. Jungen and D. Dill, J. Chem. Phys. **73**, 3338 (1980).
[42] A. Giusti-Suzor, J. N. Bardsley, and C. Derkits, Phys. Rev. A **28**, 682 (1983).
[43] V. Kokoouline and C. H. Greene, Phys. Rev. A **68**, 012703 (2003).
[44] A. Giusti, J. Phys. B: At. Mol. Phys. **13**, 3867 (1980).
[45] O. Motapon, M. Fifirig, A. Florescu, F. W. Tamo, O. Crumeyrolle, G. Varin-Bréant, A. Bultel, P. Vervisch, J. Tennyson, and I. Schneider, Plasma Sources Sci. Technol. **15**, 23 (2005).
[46] J. Z. Mezei, R. Backodissa-Kiminou, D. Tudorache, V. Morel, K. Chakrabarti, O. Motapon, O. Dulieu, J. Robert, W.-Ü. L. Tchang-Brillet, A. Bultel *et al.*, Plasma Sources Sci. Technol. **24**, 035005 (2015).
[47] M. Sommavilla, F. Merkt, J. Z. Mezei, and C. Jungen, J. Chem. Phys. **144**, 084303 (2016).
[48] C. Jungen, *Molecular Applications of Quantum Defect Theory* (Institute of Physics, Bristol, UK, 1996).
[49] D. R. Bates and L. Spitzer Jr., Astrophys. J. **113**, 441 (1951).
[50] M. Krauss and P. Jlienne, Astrophys. J. **183**, L139 (1973).
[51] A. Giusti-Suzor and H. Lefebvre-Brion, Astrophys. J. **214**, L101 (1977).
[52] A. Douglas and G. Herzberg, Astrophys. J. **94**, 381 (1941).
[53] W. S. Adams, Astrophys. J. **93**, 11 (1941).
[54] K. Hassouni, F. Silva, and A. Gicquel, J. Phys. D. **43**, 153001 (2010).
[55] https://euro-fusion.org/jet/
[56] H. Takagi, N. Kosugi, and M. Le Dourneuf, J. Phys. B: At., Mol. Opt. Phys. **24**, 711 (1991).
[57] E. Chang and U. Fano, Phys. Rev. A. **6**, 173 (1972).
[58] C. H. Greene and C. Jungen, Adv. At. Mol. Phys. **21**, 51 (1985).
[59] M. Aymar, C. H. Greene, and E. Luc-Koenig, Rev. Mod. Phys. **68**, 1015 (1996).
[60] J. Tennyson, Phys. Rep. **491**, 29 (2010).
[61] M. J. Seaton, Rep. Prog. Phys. **46**, 167 (1983).
[62] V. Kokoouline, A. Faure, J. Tennyson, and C. H. Greene, Mon. Not. R. Astron. Soc. **405**, 1195 (2010).
[63] M. Ayouz and V. Kokoouline, Atoms **4**, 30 (2016).
[64] M. Khamesian, M. Ayouz, J. Singh, and V. Kokoouline, Atoms **6**, 49 (2018).
[65] M. Ayouz and V. Kokoouline, Atoms **7**, 67 (2019).
[66] H.-J. Werner, P. J. Knowles, G. Knizia, F. R. Manby, and M. Schütz, WIREs Comput. Mol. Sci. **2**, 242 (2012).
[67] V. Kokoouline, O. Dulieu, R. Kosloff, and F. Masnou-Seeuws, J. Chem. Phys. **110**, 9865 (1999).
[68] Z. Biglari, A. Shayesteh, and A. Maghari, Comput. Theor. Chemy. **1047**, 22 (2014).
[69] J. M. Carr, P. G. Galiatsatos, J. D. Gorfinkiel, A. G. Harvey, M. A. Lysaght, D. Madden, Z. Masin, M. Plummer, J. Tennyson, and H. N. Varambhia, Eur. Phys. J. D **66**, 58 (2012).
[70] J. Tennyson, D. B. Brown, J. J. Munro, I. Rozum, H. N. Varambhia, and N. Vinci, J. Phys. Conf. Ser. **86**, 012001 (2007).